RSC Advances

PAPER

View Article Online
View Journal | View Issue

Cite this: *RSC Adv.*, 2024, **14**, 26152

Optimization of culture conditions of *Scenedesmus* sp. algae and catalytic performance of a $NiFe_2O_4$@SiO_2/MgO magnetic nano-catalyst for biodiesel production†

Peyman Abazari,[a] Saeed Masoum *[a] and Seyed Ali Hosseini Tafreshi[b]

This study aims to optimize the lipid content of *Scenedesmus* sp. for high-yield biodiesel production. Three factors affecting the culture conditions, namely salinity, nitrogen concentration, and light intensity, were selected and their effects on the maximum lipid content were investigated using the Box Behnken design. The results showed that the maximum lipid content (32.7% of algal dry weight) was obtained in the algal samples cultured under the optimized conditions. A core–shell magnetic nano-catalyst, $NiFe_2O_4$@SiO_2/MgO, was synthesized and used to produce biodiesel *via* the transesterification reaction. The nano-catalyst was characterized by field emission scanning electron microscopy (FE-SEM), energy-dispersive X-ray spectroscopy (EDS), X-ray powder diffraction analysis (XRD), vibrating sample magnetometry (VSM), elemental mapping techniques, transmission electron microscopy (TEM), and Fourier transform infrared spectroscopy (FT-IR). Using the Box Behnken design and keeping the temperature constant, the molar ratio of methanol to oil, the amount of catalyst, and the time were optimized to achieve the maximum yield of biodiesel. The maximum yield of biodiesel was 95.3% under the optimal conditions.

Received 19th April 2024
Accepted 15th August 2024

DOI: 10.1039/d4ra02904f

rsc.li/rsc-advances

1. Introduction

Alternative fuels are being sought instead of fossil fuels due to increasing air pollution, acid rain, and greenhouse gases.[1] It is possible to substitute fossil fuels with biofuels, such as biodiesel. Compared to gasoline, they emit fewer carbon dioxide emissions, have higher flash points, include fewer sulfur compounds, and have higher cetane numbers.[2] Sources of biofuel production are divided into four generations. Biofuel production has been able to surpass edible and non-edible seeds with microalgae in the third generation. Compared to plants, this generation grows faster, doesn't require fertile soil and freshwater, and can withstand bad environments. Microalgae can grow in saline water as well as wastewater.[3] One of the well-known algae with suitable lipid content for biodiesel production is *Scenedesmus* algae.[4] This algae was first discovered by Turpin in 1828. *Scenedesmus* is a flat colony with 2–32 cells in one or two rows. This algae has different cell shapes but is often cylindrical and lunate.[5] Biodiesel is a mono-alkyl ester produced by reacting algae oil with methanol and an acid or alkali catalyst *via* esterification or transesterification.[6] Chemical reactions can be accelerated using substances called catalysts, which do not get depleted during the process. Catalysts come in different forms like solid, liquid, and biocatalysts. Among them, magnetic solid catalysts are preferred by scientists because they have a high recovery capacity and can be quickly separated from the reaction.[7] Different methods for extracting oil from algae can be used depending on the laboratory facilities. These methods include supercritical fluid extraction, organic solvent extraction, microwave-assisted organic solvent extraction, ultrasound-assisted organic solvent extraction, and organic solvent extraction with Soxhlet apparatus.[8] The amount of lipid content in algal cells is essential for biodiesel production. Algae usually do not have a significant amount of oil but at the different route, such as some abiotic stress, can increase the amount of algae oil. These abiotic stresses like salinity, metal stress, light, and nitrogen depletion can induce lipid productivity in algal cells.[9] Ji *et al.* conducted research on *Scenedesmus obliquus* algae by adding varying amounts of NaCl to the culture medium at concentrations of 0, 0.01, 0.10, 0.15, and 0.20 M. After analyzing the data, it was found that the algae growth medium with 0.2 M of NaCl produced the highest oil yield, amounting to 32.26% of dry weight.[10] Also, Nzayisenga *et al.* stated that the effect of three light intensities of 2700, 8100, and 16 200 lux on three algae *Chlorella vulgaris*, *Desmodesmus* sp.,

[a]*Department of Analytical Chemistry, Faculty of Chemistry, University of Kashan, Kashan, Iran. E-mail: masoum@kashanu.ac.ir; Fax: +983155912397; Tel: +983155912338*

[b]*Department of Biotechnology, Faculty of Chemistry, University of Kashan, Kashan, Iran*

† Electronic supplementary information (ESI) available. See DOI: https://doi.org/10.1039/d4ra02904f

Table 1 Three levels of independent variables and experimental ranges of lipid optimization

Variable	Factor	Range and level		
		Low level (−1)	Central point (0)	High level (+1)
Light intensity (lux)	*A*	800	5000	15 000
Nitrate concentration (mM)	*B*	0.5	2.5	5
Salinity concentration (mM)	*C*	0.5	100	500

Table 2 Three levels of independent variables and experimental ranges of biodiesel optimization

Variable	Factor	Range and level		
		Low level (−1)	Central point (0)	High level (+1)
Methanol to oil molar ratio	*A*	6	12	18
Amount of catalyst (% wt)	*B*	0.5	2	4
Time (min)	*C*	60	120	180

and *Scenedesmus obliquus*, and different results were obtained, so that in *Scenedesmus* and *Desmodesmus* increasing the light intensity from 2700 to 16 200 lux increased oil production, while in *Chlorella vulgaris*, increasing the light intensity decreased oil production in algae cells.[11]

Response surface methodology (RSM) is a statistical and mathematical method to optimize different and important factors in the response of an experiment.[12] The big advantage of RSM is that it helps us get optimal solutions faster with fewer test runs.[13] There are various methods for experimental designs. The most common of which are Box Behnken design, central composite design, full factorial design. Box–Behnken design (BBD) is a design that, unlike central composite design, which is done on five levels, is done only on three levels (−1, 0, +1), which increases the economic advantage of this method compared to central composite design.[14]

Nanocomposites have various applications, among these applications, their use as battery cathodes, nanowires, sensors, non-linear optics, and other systems can be mentioned.[15] One of the latest applications of nanocomposites is the use of highly active ZIF-8@CNT composite catalysts as cathode materials for anion exchange membrane fuel cells.[16]

In 2019, Arul Raj *et al.* were able to produce biodiesel with a yield of 87.5% by using an optimized process. They achieved this by synthesizing a nano-catalyst made of polyethylene glycol (PEG) encapsulated $ZnOMn^{2+}$ and extracting oil from the algae *Nanochloropsis ocutala*. The optimal conditions for this process were a 15 : 1 molar ratio of methanol to oil, 4 hours reaction time, 60 °C reaction temperature, and 3.5 wt% catalyst amount.[17] Also, the optimal amount of 4% calcium oxide nano-catalyst showed the highest efficiency in producing biodiesel using *Chlorella vulgaris* algae oil in a transesterification reaction.[18]

In 2022, Farrokheh *et al.* conducted a study to determine the effectiveness of two magnetic nanocatalysts, CaO/KOH–Fe_3O_4, and KF/KOH–Fe_3O_4, on the oil extracted from two types of algae, *Chlorella vulgaris* and *Spirulina platensis*. The goal of the study was to produce biofuel using the electrolysis method. Results showed that the oil extracted from *Chlorella vulgaris* and the KF/KOH–Fe_3O_4 magnetic nano-catalyst had the best performance under optimal conditions. These conditions included a molar ratio of methanol to oil of 6 : 1, a reaction time of 2 hours, a catalyst amount of 1.5 wt%, and a reaction temperature of 25 °C. The reaction yield was found to be 96.8%.[19] Also in 2023, Mittal and Gash successfully created biodiesel with a 99% yield. They accomplished this by using a calcium methoxide nano-catalyst and oil from *Spirulina* algae during the trans-esterification reaction. The optimal conditions for this process were a 30 : 1 molar ratio of methanol to oil, 3 wt% of catalyst, 3 hours reaction time, and a temperature of 80 °C.[20]

This study focused on using *Scenedesmus* sp. to produce high-yield biodiesel, synthesis of a nickel ferrite nano-catalyst coated with silica and functionalized with magnesium oxide, characterization of magnetic catalyst, investigation of magnetic catalyst in trans-esterification of *Scenedesmus* sp. to produce high-yield biodiesel and optimizing the conditions of process using BBD. The magnetic core in the synthesized catalyst increases its recycling properties and enables easy separation from the reaction environment. The core–shell structure serves to safeguard the magnetic core from physical and chemical

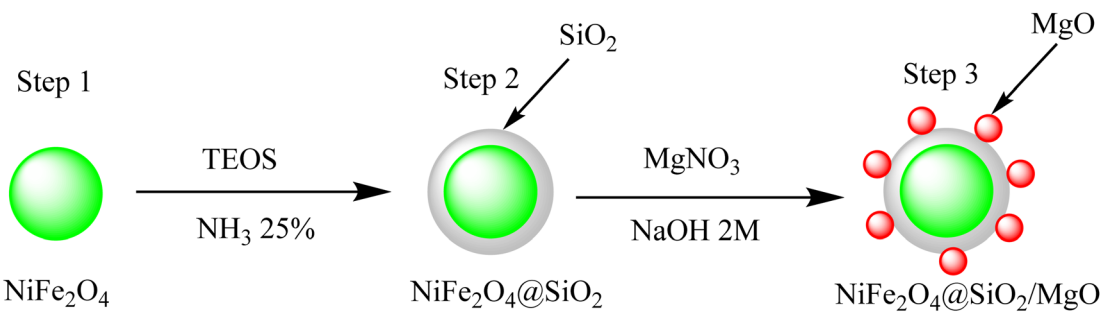

Fig. 1 Stepwise preparation of $NiFe_2O_4@SiO_2/MgO$ core–shell magnetic nano-catalyst.

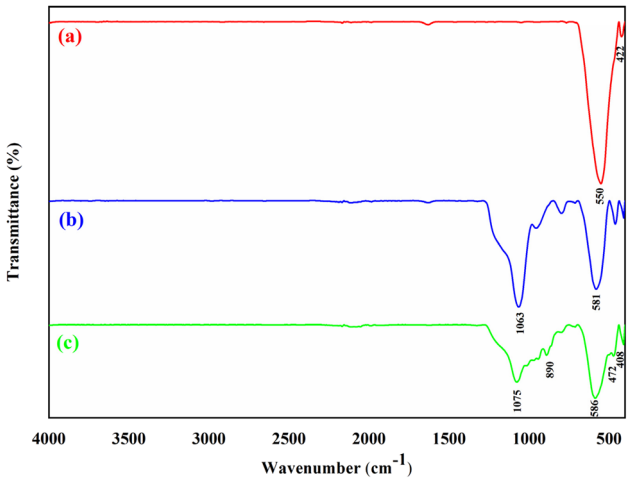

Fig. 2 The FT-IR spectra of $NiFe_2O_4$ (a), $NiFe_2O_4$@SiO_2 (b), and $NiFe_2O_4$@SiO_2/MgO (c).

damage. Magnesium oxide nanoparticles are used for their high stability in environmental conditions and their good track record in previous research.[21,22]

2. Experimental section

2.1. Materials

All chemicals were purchased from Merck (Germany) and used as received without further purification.

Synthesis of $NiFe_2O_4$@SiO_2/MgO

Synthesis of $NiFe_2O_4$. To synthesize the nickel ferrite magnetic nano-catalyst, start by adding 50 ml of 0.4 M $FeCl_3 \cdot 6H_2O$ solution to 50 ml of 0.2 M $NiCl_2 \cdot 6H_2O$ solution. Pour both solutions into a round-bottom flask and heat it to 50 °C. After 15 minutes, NaOH 3 M was added drop by drop until the pH of the environment reached 13, then 3 drops of oleic acid were added and stirred for 50 minutes at a temperature of 80 °C. During this period, to prevent iron from oxidizing, nitrogen was purged inside the flask. The obtained sediments were washed three times with deionized water and ethanol and then dried in an oven at 80 °C for 12 hours. Finally, they were calcined at 600 °C for 10 hours.[23]

Synthesis of $NiFe_2O_4$@SiO_2. One gram of synthesized nickel ferrite in the previous step was weighed. The mixture of 20 ml of ethanol and 4 ml of deionized water was added to it and was placed under nitrogen gas for 5 minutes in the mechanical recoil, then 1 ml of tetraethoxysilane (TEOS) and 2 ml of 25% ammonia was added to the reaction mixture. The reaction was carried out under room temperature for 3 hours. Finally, the resulting product was separated with an external magnet washed three times with deionized water and ethanol, and dried at a temperature of 70 °C for 8 hours.[24]

Synthesis of $NiFe_2O_4$@SiO_2/MgO. To synthesize $NiFe_2O_4$@SiO_2/MgO, Rahimi *et al.*'s method was used with slight modifications,[25] so that a solution of 60% (w/w) of magnesium nitrate to $NiFe_2O_4$@SiO_2 was prepared. After stirring 1 gr of $NiFe_2O_4$@SiO_2 in the solution above at 40 °C for 1 hour sodium hydroxide (2 M) was added drop by drop until the pH reaches

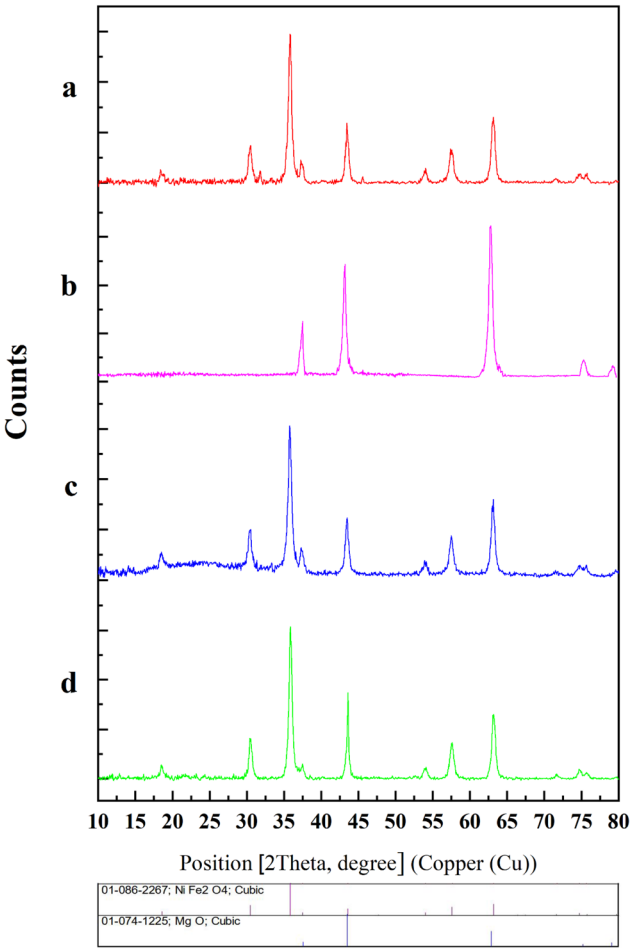

Fig. 3 The XRD pattern of $NiFe_2O_4$ (a), MgO (b), $NiFe_2O_4$@SiO_2 (c), and $NiFe_2O_4$@SiO_2/MgO (d).

11–12, and stir for an additional hour at 65 °C. Then the obtained sediment was washed three times with distilled water and dried for 10 hours at 80 °C in an oven and finally calcined at 650 °C for 2.30 hours.

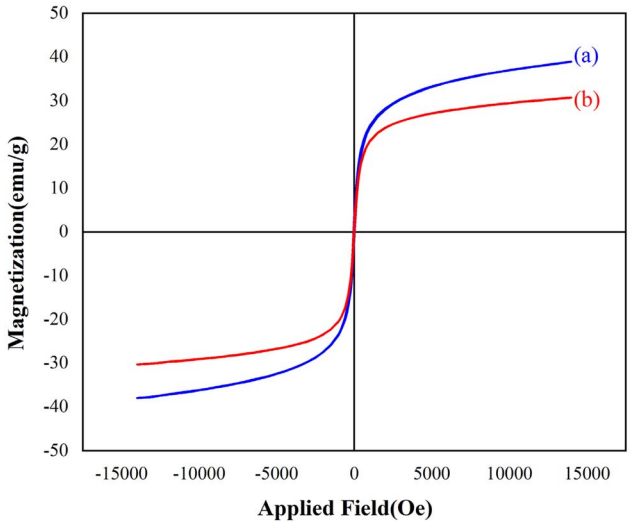

Fig. 4 The VSM analysis of $NiFe_2O_4$ (a) and $NiFe_2O_4$@SiO_2/MgO (b).

Table 3 The nanoparticles' peak position, full width at half maximum ($\beta\frac{1}{2}$), and calculated crystal size of $NiFe_2O_4$@SiO_2/MgO

Peak position 2θ (°)	30.46	35.86	43.54	57.60	63.19
FWHM β (°)	0.29	0.41	0.35	0.35	0.29
Size (nm)	29.67	21.28	25.54	27.07	33.61

$\lambda = 0.154$ nm, $K = 0.94$

2.2. Instrumentation

The IR spectra were recorded on an ATR Bruker Tensor II (Germany) in the range of 400–4000 cm^{-1}. A Philips instrument with Cu anode ($\lambda = 0.154056$ nm) was used to record XRD patterns of the synthesized catalyst from 10° to 80° (2θ). Field emission scanning electron microscopy (FE-SEM) of the nano-catalyst was conducted using a TESCAN MIRA 3 (Czech Republic) at a 15 kV accelerating voltage. The magnetic properties of the produced nano-catalyst were evaluated using the MDKB instrument from Iran. The morphological features of the sample were investigated with a Zeiss (Germany) Transmission Electron Microscope (TEM) operating at 100 kV. The optical density of the algae sample was measured using OPTIZEN 3220UV (South Korea), and the identification of FAMEs was carried out using GC-MS equipment (GC 6890, MS 5973 from Agilent (USA)).

2.3. Microalgal culture conditions

Scenedesmus sp. was obtained from algal culture collection of University of Kashan. The alga was cultured and maintained in Johnson medium (0.5 mM NaCl) in sterile conditions at 25 °C and under 1500 lux light intensity with a photoperiod of 12 : 12 hours of dark : light cycles.[26]

2.4. Experimental design of lipid content and trans-esterification reaction

To optimize the amount of lipid in *Scenedesmus*, the response surface methodology (RSM) based on Box–Behnken design (BBD) was used. Design-Expert software (Ver. 13.0.5.0) designed 15 experiments with 3 central points according to the following equation.[27]

$$N = 2k(k - 1) + C_0 \quad (1)$$

In this equation N is the number of experiments, k is the number of factors and C_0 represents the number of times the central point repeats.

After investigating the factors affecting lipid production, three factors were selected. Light intensity (A), nitrate concentration (B), and salinity (C), were arranged in three levels (−1, 0, +1) (see Table 1). These factors were applied to the algal growth media on the 14th day of culture when the algae located at logarithmic phase of growth. 5 days after treating, the amount of lipid was measured.

Box–Behnken design can be fitted to the quadratic model to show the interactive effects between the experimental variables to optimize the factors that affect the yield of lipid production for achieving a high yield of lipid production. The following quadratic equation model can be expressed.[28]

$$Y = \alpha_0 + \alpha_1 A + \alpha_2 B + \alpha_3 C + \alpha_4 AB + \alpha_5 AC + \alpha_6 BC + \alpha_7 A^2 + \alpha_8 B^2 + \alpha_9 C^2 + \varepsilon \quad (2)$$

Y = % lipid or biodiesel yield, α_0 = intercept value, α_{1-3} = main effect, α_{4-6} = interaction effect, α_{7-9} = quadratic effect, ε = random error.

For the trans-esterification reaction three factors such as: methanol to oil molar ratio (A), amount of catalyst (B), time (C), were chosen to optimize the yield of biodiesel production at constant temperature (60 °C). The range and level of these factors are displayed in Table 2. According to Design-Expert software, 15 experiments with 3 central points were run. During the designed experiment, each test was conducted inside a round-bottom balloon equipped with a mechanical stirrer, a condenser, and a heater. After the reaction, an external magnet removed the catalyst and the mixture was separated in a funnel into the upper phase (biodiesel) and bottom phase (glycerol) as a byproduct of the trans-esterification reaction. Biodiesel yield was calculated according to eqn (3). Also, in this case, eqn (2) as a quadratic equation was used to show the interactive effects between independent variables and optimization of biodiesel production yield.[18]

$$\text{Biodiesel yield} = \frac{\text{weight of biodiesel}}{\text{weight of lipid content}} \times 100 \quad (3)$$

2.5. Algal growth

Optical densities of the control and 15 different samples at 750 nm were read by UV/Vis spectrophotometer at various time points. The specific growth rate (μ) was also calculated based on the following equation:[29]

$$\mu = \frac{\ln\left(\frac{X_2}{X_1}\right)}{t_2 - t_1} \quad (4)$$

In this case, X_1 and X_2 were the OD_{750} at t_1 and t_2 (day of measurment), respectively.

2.6. Lipid content

To measure the lipid content of *Scenedesmus* algae, the modified method of Bligh and Dyer was used.[30] Chloroform and methanol were added to 1 g of dry algae powder in a ratio of 2 : 1, so that the first 5 ml of chloroform and 5 ml of methanol were added to the dry algae powder, and vortexed for 5 minutes, then another 5 ml of chloroform was added to the algae sample and vortexed again for five minutes. After that, for better separation of chloroform and methanol, 10 ml of sodium chloride 1% (w/w) was added to the above sample, and the sample was centrifuged for 15 minutes at a speed of 6000 rpm. After centrifuge, chloroform and methanol are completely separated, the upper phase is the methanol and the lower one is the chloroform, which contains the lipid content. The chloroform content was poured into a pre-weighed test tube and placed in the oven for 24 hours at a temperature of 55 °C. The percentage of lipid content was calculated according to the following equation:

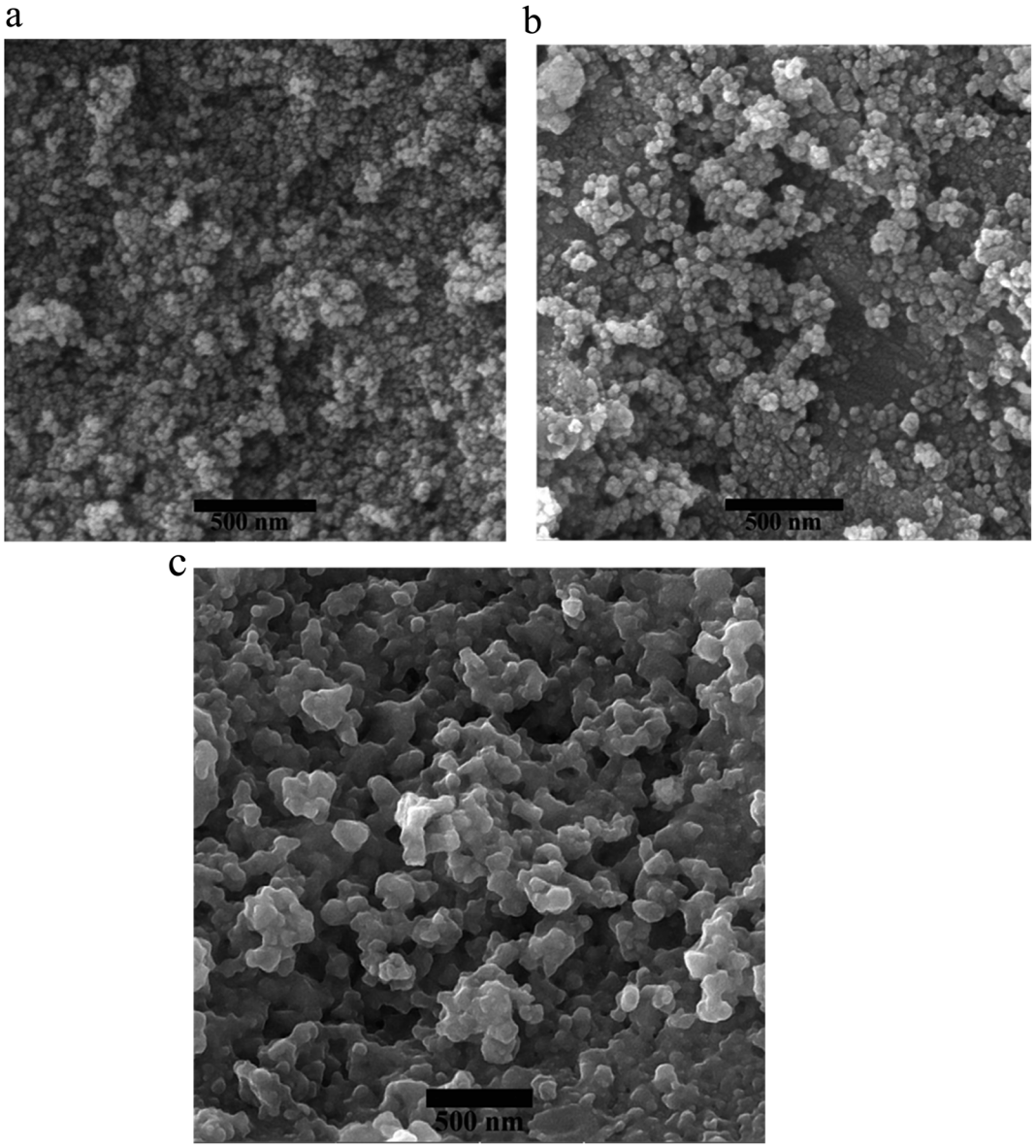

Fig. 5 FE-SEM images of the $NiFe_2O_4$ (a), $NiFe_2O_4$@SiO_2 (b) and $NiFe_2O_4$@SiO_2/MgO (c).

$$\%\ \text{Lipid} = \frac{\text{weight of lipid}}{\text{weight of dry biomass}} \times 100 \quad (5)$$

2.7. GC-MS analysis of produced biodiesel by $NiFe_2O_4$@SiO_2/MgO

The total extracted lipids from *Scenedesmus* sp. were converted to fatty acid methyl esters (FAMEs) by treating methanol and synthesized catalyst in the optimized condition in trans-esterification reaction at 60 °C. For analyzing FAMEs, gas chromatography-mass spectroscopy with HP-5ms capillary column (60 m × 250 μm × 0.25 μm) was used. 1 μl of FAMEs sample was injected at 250 °C in splitless mode. The temperature of the oven was initially maintained at 50 °C without holding time and increased to 250 °C at a ramping of 3 °C min^{-1}, and hold for 5 min at this temperature. By analyzing retention times and library search reports (NISTIL.S database), identification of FAMEs was performed.

3. Result and discussion

3.1. Characterization of $NiFe_2O_4$@SiO_2/MgO core–shell magnetic nano-catalyst

$NiFe_2O_4$@SiO_2/MgO core–shell magnetic nano-catalyst was synthesized in three main steps as shown in Fig. 1. In the first step $NiFe_2O_4$ was synthesized by the co-precipitation method. In the second step, a layer of silica was coated on the surface of the nickel ferrite synthesized in the previous step. The synthesized nano-catalyst was finally modified with MgO on its surface for functionalization. The core–shell magnetic nano-catalyst was characterized by FT-IR, XRD, VSM, FE-SEM and TEM.

The FT-IR spectrum of $NiFe_2O_4$ (a), $NiFe_2O_4$@SiO_2 (b), and $NiFe_2O_4$@SiO_2/MgO (c) in the range 400–4000 cm^{-1} is shown in

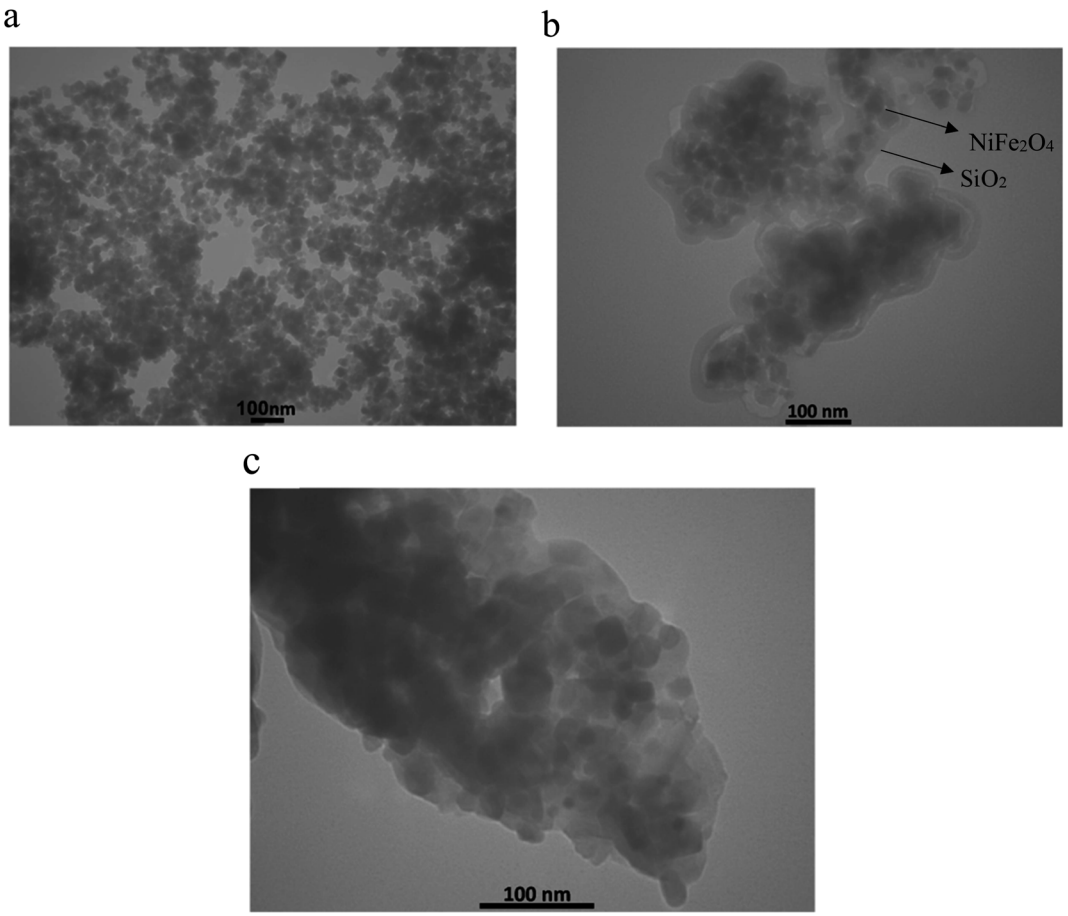

Fig. 6 TEM images of the $NiFe_2O_4$ (a), $NiFe_2O_4$@SiO_2 (b) and $NiFe_2O_4$@SiO_2/MgO (c).

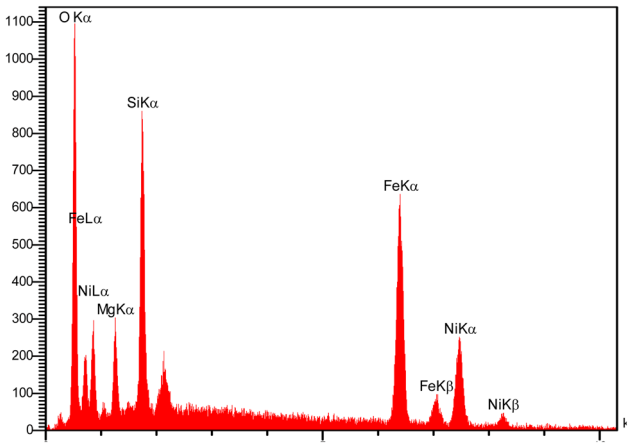

Fig. 7 EDS spectrum of the $NiFe_2O_4$@SiO_2/MgO.

Fig. 2. The bands at 550 and 422 cm^{-1} are related to the stretching vibration of Fe–O and Ni–O, respectively (Fig. 2a).[31] For all three steps, the related peaks of $NiFe_2O_4$ were observed at 408–586 cm^{-1}. The peaks at 1075 cm^{-1} and 1063 cm^{-1} in Fig. 2b and c are attributed to the Si–O–Si stretching vibration that shows silica coated on the surface of nickel ferrite.[32] The peak at 472 cm^{-1} is assigned to Mg–O–Si vibration.[33] The MgO cubic face peak is exhibited at 890 cm^{-1}.[34]

The XRD patterns of $NiFe_2O_4$ (a), MgO (b), $NiFe_2O_4$@SiO_2 (c), and $NiFe_2O_4$@SiO_2/MgO (d) are presented in Fig. 3. $NiFe_2O_4$, $NiFe_2O_4$@SiO_2 XRD patterns are matched with standard characteristic peaks reported in JCPDS card number 01-086-2267. Also $NiFe_2O_4$@SiO_2/MgO XRD pattern is matched with card number 01-074-1225. The characteristic peak at $2\theta = 25°$ shows that amorphous SiO_2 coated on the surface of nickel ferrite successfully.

The synthesized $NiFe_2O_4$, $NiFe_2O_4$@SiO_2, and $NiFe_2O_4$@SiO_2/MgO nanoparticles had a crystallite size of 18.96, 26.73, and 27.43 nm, respectively, according to the Debye Scherrer formula and information related to Debye Scherrer calculation for $NiFe_2O_4$, $NiFe_2O_4$@SiO_2, and $NiFe_2O_4$@SiO_2/MgO are shown in Tables S1, S2† and 3, respectively.[35]

$$D = \frac{K\lambda}{\beta \cos \theta} \quad (6)$$

D = crystal size (nm), K and λ = constant, β = peak width at half height.

The magnetic properties of $NiFe_2O_4$ (a) and $NiFe_2O_4$@SiO_2/MgO (b) are shown in Fig. 4. The magnetic properties of $NiFe_2O_4$ were detected at 38.94 emu g^{-1} while after coating with SiO_2 and functionalizing with MgO magnetic properties of the synthesized nano-catalyst reached 30.76 emu g^{-1} with a decrease of

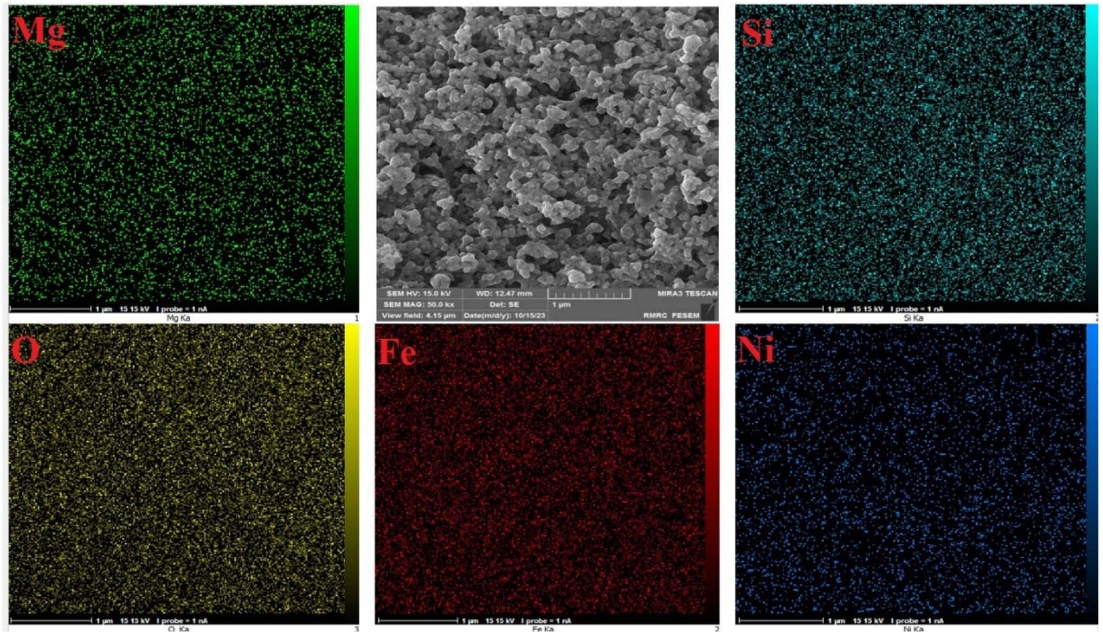

Fig. 8 Picture of the elemental mapping of the $NiFe_2O_4$@SiO_2/MgO.

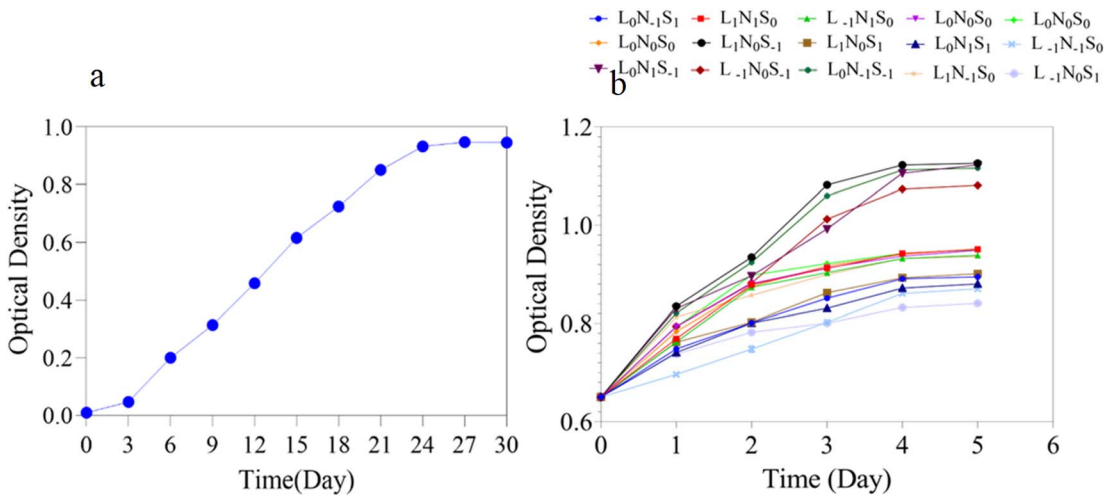

Fig. 9 The growth curve of the control medium (a) and 15 treatments (b) for lipid content optimization. (L, N, and S are related to light intensity, nitrate concentration, and salinity, respectively, and −1, 0, 1 is related to levels of experiments).

about 8.18 emu g^{-1}. The findings suggest that the magnetic nano-catalyst that was synthesized has robust magnetic properties, which enable effortless separation from the reaction mixture by utilizing an external magnet. This feature enhances the economic viability of the reaction by allowing the catalyst to be reused multiple times.

FE-SEM analyses were employed to examine the synthesized nanoparticles' size and morphology, as shown in Fig. 5. The average nanoparticle size for $NiFe_2O_4$ (Fig. 5a), $NiFe_2O_4$@SiO_2 (Fig. 5b), and $NiFe_2O_4$@SiO_2/MgO (Fig. 5c) was determined to be 16, 25, and 40 nm. As depicted in the SEM image of the final catalyst, the three-dimensional structure and the voids between the manufactured nano-catalyst have increased the surface area of contact with the environment, leading to a significant increase in the efficiency and effectiveness of the catalyst.

The TEM image of $NiFe_2O_4$ (a), $NiFe_2O_4$@SiO_2 (b), and $NiFe_2O_4$@SiO_2/MgO (c) was demonstrated in Fig. 6. As shown in Fig. 6b the structure of core and shell is well represented. Fig. 6c was related to the final catalyst, showing a weaker core and shell structure due to the deposition of magnesium oxide nanoparticles on the silica surface.

The elemental energy-dispersive X-ray (EDS) spectrum of the $NiFe_2O_4$@SiO_2/MgO nano-catalyst is displayed in Fig. 7. This nano-catalyst contains Si, Fe, Ni, Mg, and O with the following weight percentages according to the spectrum; Si: 8.81 (% w/w), Fe: 34.86 (% w/w), Ni: 23.31 (% w/w), Mg: 3.91 (% w/w), and O:

Table 4 The specific growth rate of the control sample and 15 treatments for lipid content optimization

Sample	μ (d^{-1})	Sample	μ (d^{-1})	Sample	μ (d^{-1})	Sample	μ (d^{-1})
Control	0.090	$L_0N_0S_0$	0.082	$L_0N_1S_1$	0.077	$L_1N_{-1}S_0$	0.062
$L_0N_{-1}S_1$	0.060	$L_0N_0S_0$	0.079	$L_0N_1S_{-1}$	0.100	$L_0N_0S_0$	0.081
$L_1N_1S_0$	0.070	$L_1N_0S_{-1}$	0.111	$L_{-1}N_0S_{-1}$	0.106	$L_{-1}N_{-1}S_0$	0.076
$L_{-1}N_1S_0$	0.077	$L_1N_0S_1$	0.052	$L_0N_{-1}S_{-1}$	0.119	$L_{-1}N_0S_1$	0.059

Table 5 Analysis of variance for the reduced quadratic model (coded units) for the lipid content

Source	Sum of squares	df	Mean square	*F*-Value	*p*-Value	
Model	516.35	7	73.76	72.28	<0.0001	Significant
A-Light intensity	38.06	1	38.06	37.30	0.0005	
B-Nitrate concentration	51.16	1	51.16	50.13	0.0002	
C-Salinity	304.80	1	304.80	298.67	<0.0001	
AB	5.55	1	5.55	5.43	0.0525	
BC	10.18	1	10.18	9.97	0.0160	
B^2	83.22	1	83.22	81.55	<0.0001	
C^2	29.98	1	29.98	29.38	0.0010	
Residual	7.14	7	1.02			
Lack of fit	6.85	5	1.37	9.44	0.0986	Not significant
Pure error	0.2905	2	0.1452			
Cor total	523.49	14				
R-Squared	0.9864					
Adj *R*-squared	0.9727					
Pred *R*-squared	0.8884					

Table 6 Box–Behnken design and obtained response from each experiment for the lipid content

	Factor *A*	Factor *B*	Factor *C*	Percentage of lipid content	
Run	Light intensity (lux)	NO_3 (mM)	Salinity (mM)	Experimental	Predicted
1	800	0.5	100	25.8	26.4
2	5000	5	500	28.0	28.6
3	15 000	2.5	0.5	10.4	10.3
4	5000	5	0.5	12.9	13.0
5	5000	2.5	100	15.8	15.8
6	5000	0.5	500	31.2	30.5
7	800	5	100	19.8	19.0
8	15 000	2.5	500	22.6	22.6
9	5000	2.5	100	16.6	15.8
10	5000	2.5	100	16.2	15.8
11	5000	0.5	0.5	22.5	21.3
12	800	2.5	0.5	13.5	14.7
13	800	2.5	500	26.9	27.0
14	15 000	5	100	17.0	17.0
15	15 000	0.5	100	18.4	19.7

29.12 (% w/w). The small amount of Mg in the catalytic will increase the trans-esterification reaction efficiency.[36]

The elemental mapping of the $NiFe_2O_4$@SiO_2/MgO is shown in Fig. 8. These images demonstrate uniform dispersion of constituent elements throughout the synthesized nano-catalyst, creating active sites across the entire catalyst surface. As a result, the efficiency of this catalyst increases in the trans-esterification reaction.

3.2. Investigating the growth of algae in the control medium and stressed medium

The growth curves of *Scenedesmus* sp. algae under the control medium (a) and 15 treatments (b) related to the optimization of the lipid content are shown in Fig. 9, and the specific growth rate (μ) is calculated and shown in Table 4. The results of biomass measurement only showed a negligible decrease in biomass. The final biomass of the control sample was equal to 0.877 g l^{-1} and in the optimized condition with the highest amount of lipid content was equal to 0.730 g l^{-1} after five days of culture.

3.3. Result of the Box–Behnken design for optimization of the lipid content

To determine the optimum conditions for producing high lipid content, the response surface methodology and Box–Behnken design method were applied. In the first section of the design experiment, three factors (*A*: light intensity, *B*: nitrate concentration, and, *C*: salinity concentration) were chosen as the independent variables that affected lipid production, and the percentage of lipid was selected as the response. Table 5 presents ANOVA results for the influencing factors on lipid production, which shows that the factors with *p*-value < 0.05 have a significant impact on lipid production. Consequently, the *A* (light intensity), *B* (KNO_3 concentration), *C* (salinity concentration), B^2, C^2, and *BC* (NO_3 concentration × salinity concentration) have *p*-values smaller than 0.05 and significantly increased lipid productivity.

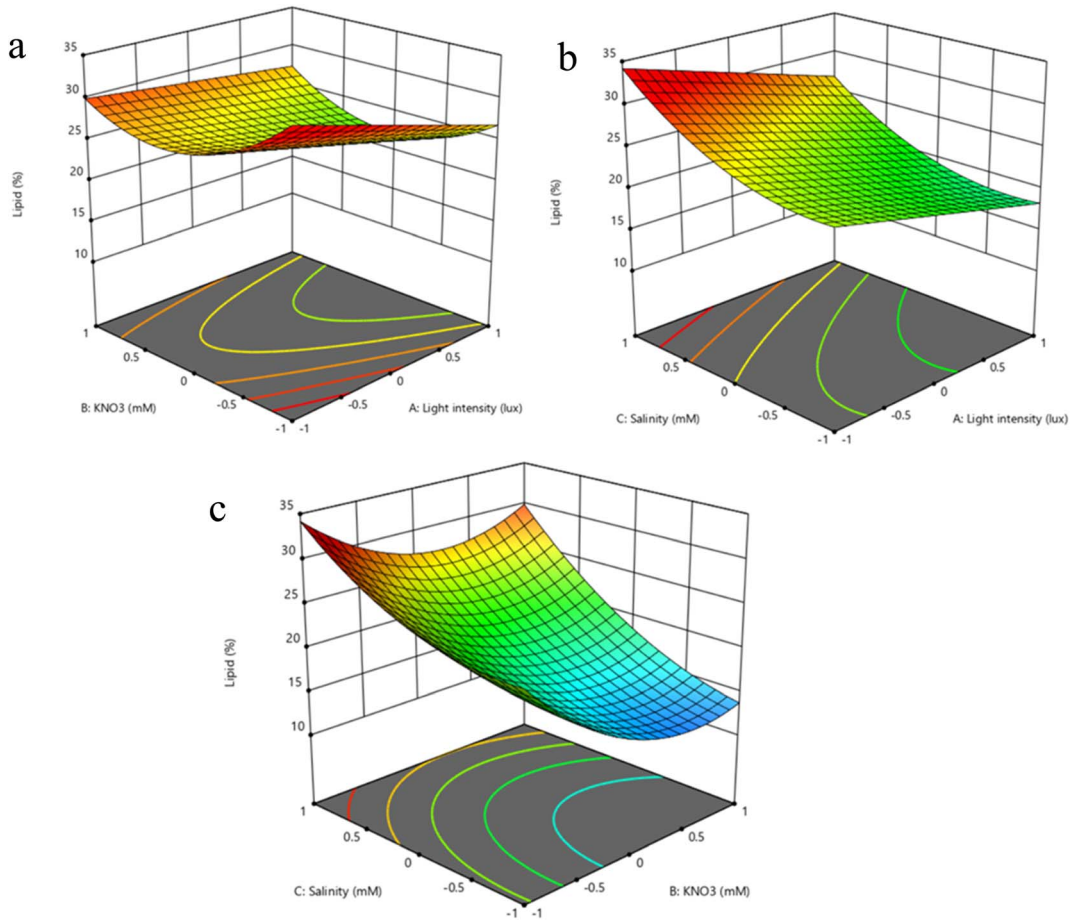

Fig. 10 The response surface plots: (a) interactive effect of light intensity and NO_3 concentration, (b) interactive effect of light intensity and salinity concentration, (c) interactive effect of NO_3 concentration and salinity concentration.

Table 7 Analysis of variance for the reduced quadratic model (coded units) for the biodiesel yield

Source	Sum of squares	df	Mean square	*F*-Value	*p*-Value	
Model	7865.62	6	1310.94	210.23	<0.0001	Significant
A-Methanol to oil	190.03	1	190.03	30.47	0.0006	
B-Amount of catalyst	896.55	1	896.55	143.77	<0.0001	
C-Reaction time	312.50	1	312.50	50.11	0.0001	
AB	59.91	1	59.91	9.61	0.0147	
A^2	5497.80	1	5497.80	881.64	<0.0001	
C^2	1250.76	1	1250.76	200.58	<0.0001	
Residual	49.89	8	6.24			
Lack of fit	47.84	6	7.97	7.80	0.1180	Not significant
Pure error	2.05	2	1.02			
Cor total	7915.51	14				
R-Squared	0.9937					
Adj *R*-squared	0.9890					
Pred *R*-squared	0.9794					

Scenedesmus sp. algae lipid content can be predicted using a reduced quadratic model using the following equation:

$$Y = 15.81 - 2.18A - 2.53B + 6.17C + 1.18AB + 1.60BC + 4.73B^2 + 2.84C^2 \quad (7)$$

In Table 6, calculated results from the reduced quadratic model are summarized based on experimental ranges and levels of independent variables.

Fig. 10 illustrates response surface plots between pairs of two experimental variables. As a result of all 15 experimental runs

Table 8 Box–Behnken design and obtained response from each experiment for the biodiesel yield

	Factor *A*	Factor *B*	Factor *C*	Biodiesel yield	
Run	Methanol to oil molar ratio	Amount of catalyst (% wt)	Reaction time (min)	Experimental	Predicted
1	6	2	180	44.7	41.7
2	6	2	60	27.5	29.2
3	12	4	180	84.3	85.9
4	18	2	60	17.1	19.4
5	12	4	60	74.3	73.4
6	12	0.5	60	55.3	52.2
7	6	0.5	120	38.7	39.3
8	12	0.5	180	61.2	64.7
9	12	2	120	87.0	87.4
10	6	4	120	67.6	68.2
11	12	2	120	87.3	87.7
12	18	4	120	50.9	50.8
13	18	0.5	120	37.4	37.3
14	18	2	180	34.0	31.9
15	12	2	120	88.9	87.4

using response surface methodology, the following conditions produce maximum lipid content (32.7% of algal dry weight): $A =$ 800 lux (light intensity), $B = 0.5$ mM (KNO_3 concentration), $C =$ 500 mM (salinity concentration).

3.4. Result of the Box–Behnken design for optimization of the biodiesel yield

During the second part of this design experiment, at a constant temperature (60 °C), three independent variables that affect the reaction conditions of biodiesel production were considered,

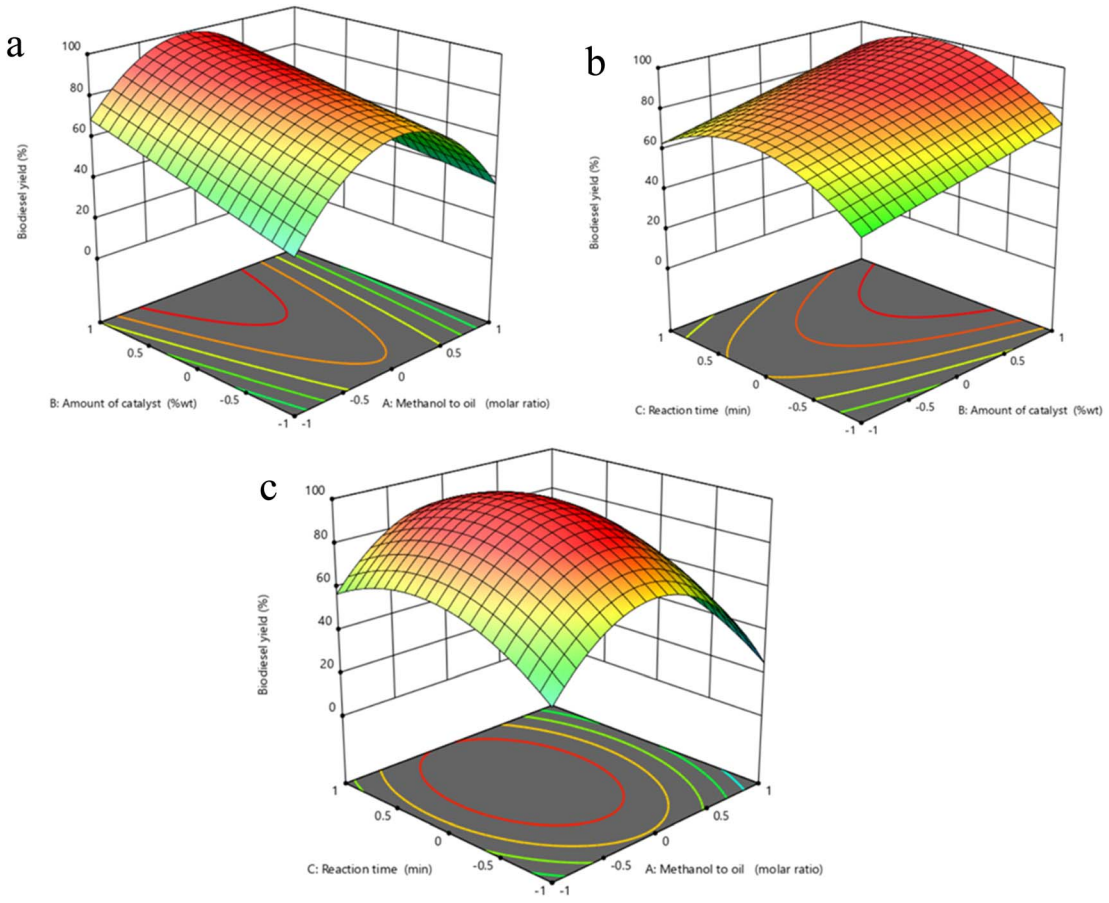

Fig. 11 Response surface plots: (a) interactive effect of methanol to oil molar ratio and amount of catalyst, (b) interactive effect of amount of catalyst and reaction time, (c) interactive effect of methanol to oil molar ratio and reaction time.

Table 9 Main FAME composition of *Scenedesmus* sp. biodiesel synthesized under optimal conditions

Number	Retention time	Compound name	Percent
1	47.8	Myristic acid, methyl ester	4.1
2	53.3	Methyl 4,7,10,13-hexadecatetranoate	7.0
3	54.0	Palmitoleic acid, methyl ester	14.0
4	54.8	Palmitic acid, methyl ester	32.7
5	60.2	Linoleic acid, methyl ester	9.0
6	60.4	Linolenic acid, methyl ester	28.6
7	60.6	Elaidic acid, methyl ester	3.5
8	60.9	Stearic acid, methyl ester	1.1

including methanol to oil molar ratio (A), amount of catalyst (B), and reaction time (C). This was accomplished by designing 15 experiments and selecting biodiesel yield as the response variable. Table 7 provides the ANOVA table for variables affecting biodiesel yield. As a result, A (molar ratio methanol to oil), B (amount of catalyst), C (reaction time), AB (molar ratio methanol to oil × amount of catalyst), A^2 and C^2 factors significantly improved biodiesel yields.

According to the Box–Behnken design and response surface methodology, eqn (8) represents the correlation between experiment variables and response (biodiesel yield, Y).

$$Y = 87.39 - 4.87A + 10.59B + 6.25C - 3.87AB - 38.47A^2 - 18.35C^2 \quad (8)$$

In Table 8, the experimental conditions and the obtained results are presented. Response surface plots between pairs of two experimental variables are shown in Fig. 11. Using response surface methodology, the following conditions have been found to produce high biodiesel yields (95.34%): $A = 11.3$ (methanol to oil molar ratio), $B = 4$ (amount of catalyst), $C = 130$ (time).

As shown in Table 9 and Fig. 12, the main FAME composition and GC-MS spectrum of *Scenedesmus* sp. biodiesel synthesized under ideal conditions were reported. The results of GC-MS analysis show that the high presence of methyl esters with carbon numbers of 16 and 18 can reduce oxidation of biodiesel and increase the storage capacity of biodiesel.[37]

As shown in Table 10 $NiFe_2O_4$@SiO_2/MgO nano-catalyst were compared with other reported catalysts.

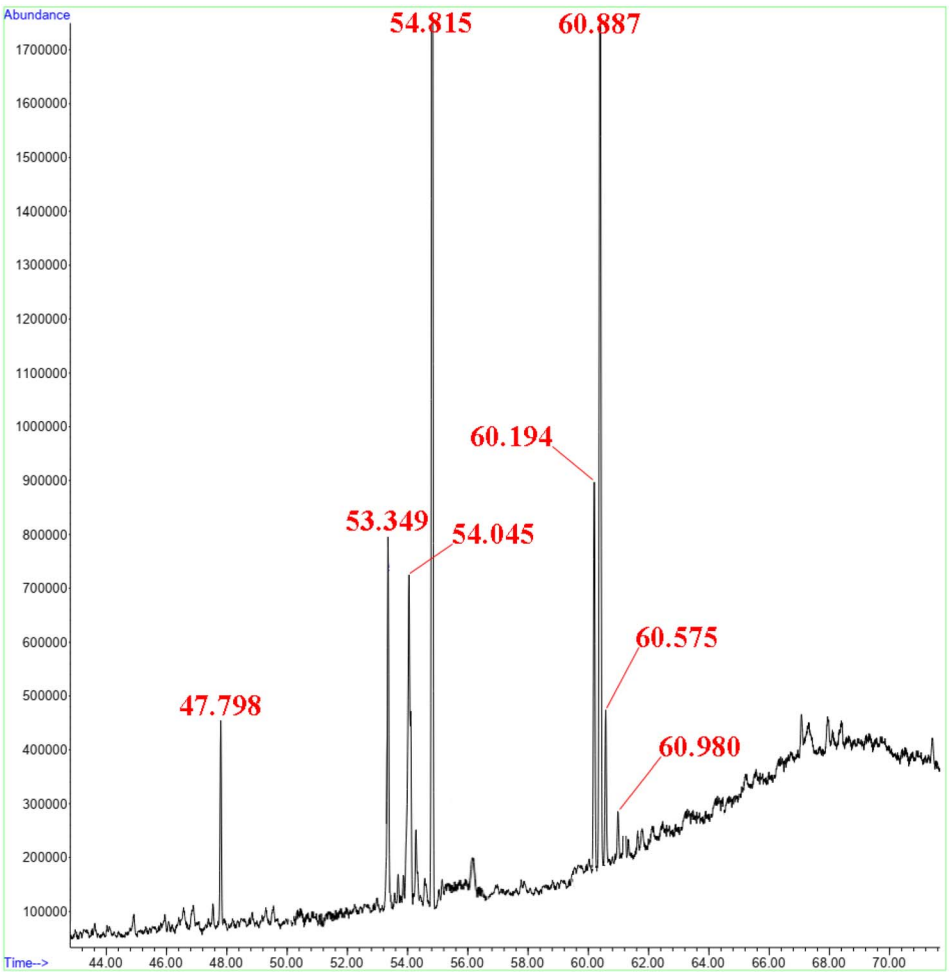

Fig. 12 GC-MS spectrum of *Scenedesmus* sp. biodiesel synthesized under optimum conditions.

Table 10 Comparison of biodiesel synthesis with $NiFe_2O_4$@SiO_2/MgO nano-catalysts other catalysts

Catalyst	Methanol to oil ratio	Amount of catalyst% (w/w)	Time (min)	Temperature (°C)	Yield (%)	Ref.
CaO	30	2.06	180	60	93.44	38
SO_4/Fe_3O_4–Al_2O_3	9	8	240	120	87.6	39
CaO	11	2	180	60	92	40
$NiFe_2O_4$@SiO_2/MgO	11.3	4	130	60	95.3	This work

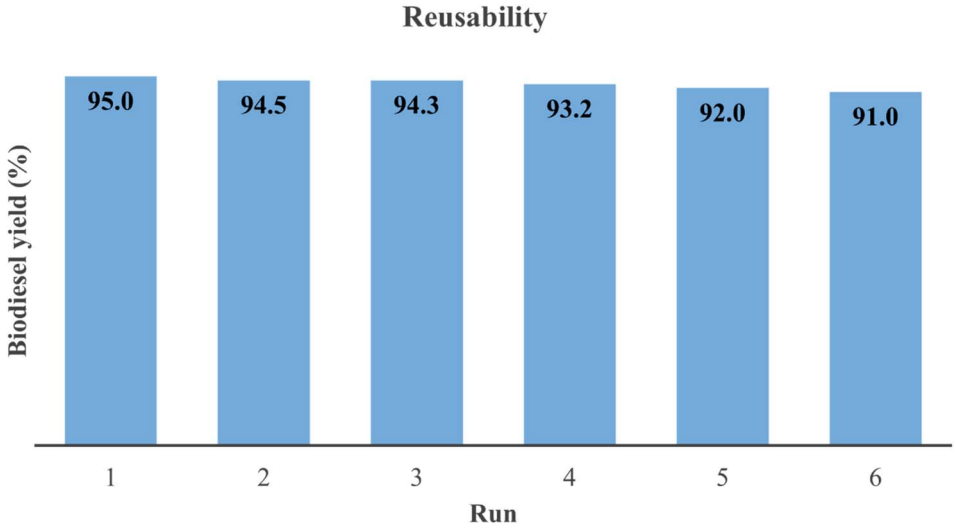

Fig. 13 The reusability of the $NiFe_2O_4$@SiO_2/MgO under optimized reaction condition.

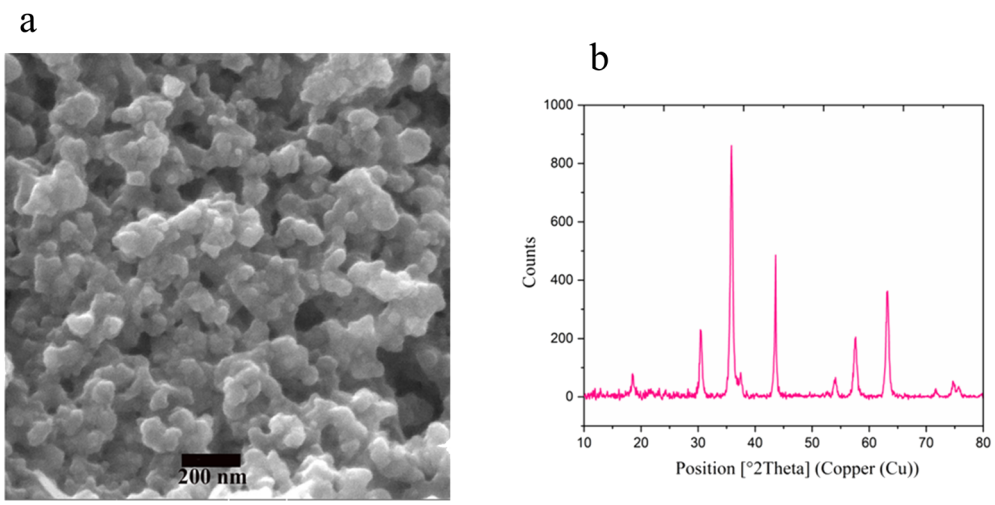

Fig. 14 FE-SEM image (a) and XRD pattern (b) of the $NiFe_2O_4$@SiO_2/MgO after recycling.

3.5. Proposed reaction mechanism of transesterification reaction

The proposed mechanism of transesterification reaction using $NiFe_2O_4$@SiO_2/MgO nano-catalyst is shown in Fig. S1.† In step 1, methanol is activated on the surface of the catalyst, and intermediate (**I**) is formed. Then, the negative charge of oxygen attacks the carbonyl group of triglyceride, and the carbonyl group is removed from the compound, therefore, methyl ester is produced (**II**). In the following, the above reaction is repeated in two consecutive steps and finally, 3 moles of methyl ester and glycerol molecule are formed (**III**).

3.6. Reusability of the $NiFe_2O_4$@SiO_2/MgO nano-catalyst

Considering the importance of environmental and economic considerations, reusable catalysts have attracted considerable attention. An attempt was made in this work to study the

reusability of a $NiFe_2O_4$@SiO_2/MgO nano-catalyst in the transesterification reaction. For this purpose, after separating the nano-catalyst by an external magnet, the catalyst was washed with acetone and deionized water and dried at 60 °C for 3 hours. This method makes the synthesized catalyst show the highest efficiency in optimized conditions with the least reduction in reaction efficiency after reuse. As shown in Fig. 13, the catalyst reusability tests were conducted after six runs.

FE-SEM image (Fig. 14a) and an XRD pattern (Fig. 14b) were obtained after several runs of $NiFe_2O_4$@SiO_2/MgO recycling and no noticeable changes in morphology and XRD patterns were observed. As evidenced by morphological and XRD patterns, the catalyst produced excellent stability and retained catalytic activity after several recovery steps.

4. Conclusion

This research aimed to optimize *Scenedesmus* sp. lipid content to produce high lipid content and high-yield biodiesel using the response surface methodology and Box–Behnken design. The catalyst used in the transesterification reaction was $NiFe_2O_4$@SiO_2/MgO. The reason for using this catalyst is the availability of cheap nanocatalyst ingredients and the high magnetic properties of this nanocatalyst, which adds to the economic features of this nanocatalyst. Also, the use of MgO due to its insensitivity to the water content of the reactants and SiO_2 due to the increase in the reaction surface, increase the efficiency of the transesterification reaction. Box–Behnken design calculations show that the results obtained from the laboratory data were accurate enough, also the efficiency of 95.3 for the production of biodiesel shows that the used catalyst has a good effect on the production of biodiesel and the transesterification reaction.

Data availability

The data supporting this article have been included as part of the ESI.†

Conflicts of interest

There are no conflicts to declare.

Acknowledgements

The authors are grateful to the University of Kashan for supporting this work by Grant No. 890412/3.

References

1 B. Changmai, C. Vanlalveni, A. P. Ingle, R. Bhagat and S. L. Rokhum, *RSC Adv.*, 2020, **10**, 41625–41679.
2 F. C. De Oliveira and S. T. Coelho, *Renewable Sustainable Energy Rev.*, 2017, **75**, 168–179.
3 B. Sajjadi, W.-Y. Chen, A. A. A. Raman and S. Ibrahim, *Renewable Sustainable Energy Rev.*, 2018, **97**, 200–232.
4 A. G. Ishaq, H. M. Matias-Peralta and H. Basri, *Pertanika J. Trop. Agric. Sci.*, 2016, **39**, 1–16.
5 E. H. Hegewald, *Algae*, 1997, **12**, 235–246.
6 D. Y. C. Leung, X. Wu and M. K. H. Leung, *Appl. Energy*, 2010, **87**, 1083–1095.
7 S. G. Krishnan, F. Pua and F. Zhang, *Biomass Bioenergy*, 2021, **149**, 106099.
8 R. Halim, M. K. Danquah and P. A. Webley, *Biotechnol. Adv.*, 2012, **30**, 709–732.
9 D. G. Giarikos, J. Brown, R. Razeghifard, D. Vo, A. Castillo, N. Nagabandi, J. Gaffney, M. Zelden, A. Antakshinova, S. Rodriguez and S. Muhammad, *Appl. Water Sci.*, 2021, **11**, 39.
10 X. Ji, J. Cheng, D. Gong, X. Zhao, Y. Qi, Y. Su and W. Ma, *Sci. Total Environ.*, 2018, **633**, 593–599.
11 J. C. Nzayisenga, X. Farge, S. L. Groll and A. Sellstedt, *Biotechnol. Biofuels*, 2020, **13**, 4.
12 M. A. Bezerra, R. E. Santelli, E. P. Oliveira, L. S. Villar and L. A. Escaleira, *Talanta*, 2008, **76**, 965–977.
13 K. Sundareswaran, S. Peddapati and S. Palani, *IET Renewable Power Generation*, 2014, **8**, 670–678.
14 S. Beg and S. Akhter, in *Design of Experiments for Pharmaceutical Product Development*, Springer Singapore, Singapore, 2021, pp. 77–85.
15 C. C. Okpala, *International Journal of Advanced Engineering and Technology*, 2014, **12**, 18.
16 R. Kumar, M. Mooste, Z. Ahmed, S. Akula, I. Zekker, M. Marandi, M. Käärik, J. Leis, A. Kikas, A. Treshchalov, M. Otsus, J. Aruväli, V. Kisand, A. Tamm and K. Tammeveski, *Ind. Chem. Mater.*, 2023, **1**, 526–541.
17 J. Vinoth Arul Raj, B. Bharathiraja, B. Vijayakumar, S. Arokiyaraj, J. Iyyappan and R. Praveen Kumar, *Bioresour. Technol.*, 2019, **282**, 348–352.
18 M. Davoodbasha, A. Pugazhendhi, J.-W. Kim, S.-Y. Lee and T. Nooruddin, *Fuel*, 2021, **300**, 121018.
19 A. Farrokheh, K. Tahvildari and M. Nozari, *Biomass Convers. Biorefin.*, 2022, **12**, 403–417.
20 V. Mittal and U. K. Ghosh, *Bioresour. Technol. Rep.*, 2023, **23**, 101504.
21 S. Alaei, M. Haghighi, B. Rahmanivahid, R. Shokrani and H. Naghavi, *Renewable Energy*, 2020, **154**, 1188–1203.
22 T. Amani, M. Haghighi and B. Rahmanivahid, *J. Ind. Eng. Chem.*, 2019, **80**, 43–52.
23 H. Naeimi and F. Kiani, *Appl. Organomet. Chem.*, 2019, **33**, 1–12.
24 A. Limouzadeh and H. Naeimi, *J. Coord. Chem.*, 2020, **73**, 1907–1924.
25 T. Rahimi, D. Kahrizi, M. Feyzi, H. R. Ahmadvandi and M. Mostafaei, *Ind. Crops Prod.*, 2021, **159**, 113065.
26 M. K. Johnson, E. J. Johnson, R. D. MacElroy, H. L. Speer and B. S. Bruff, *J. Bacteriol.*, 1968, **95**, 1461–1468.
27 G. Zhang, H. Zhang, D. Yang, C. Li, Z. Peng and S. Zhang, *Catal. Sci. Technol.*, 2016, **6**, 6417–6430.
28 A. Marwaha, P. Rosha, S. K. Mohapatra, S. K. Mahla and A. Dhir, *Energy Rep.*, 2019, **5**, 1580–1588.
29 G. E. Fogg and B. Thake, *Algal cultures and phytoplankton ecology*, University of Wisconsin Press, 1987.

30 E. G. Bligh and W. J. Dyer, *Can. J. Biochem. Physiol.*, 1959, **37**, 911–917.
31 N. Hosseini Nasab and J. Safari, *J. Mol. Struct.*, 2019, **1193**, 118–124.
32 E. Al-Bermany, A. T. Mekhalif, H. A. Banimuslem, K. Abdali and M. M. Sabri, *Silicon*, 2023, **15**, 4095–4107.
33 J. T. Kloprogge and R. L. Frost, *Vib. Spectrosc.*, 2000, **23**, 119–127.
34 T. Somanathan, V. M. Krishna, V. Saravanan, R. Kumar and R. Kumar, *J. Nanosci. Nanotechnol.*, 2016, **16**, 9421–9431.
35 M. Qiu, Y. Zhang and B. Wen, *J. Mater. Sci.: Mater. Electron.*, 2018, **29**, 10437–10444.
36 B. Rahmani Vahid, M. Haghighi, S. Alaei and J. Toghiani, *Energy Convers. Manage.*, 2017, **143**, 23–32.
37 Y. Chisti, *Biotechnol. Adv.*, 2007, **25**, 294–306.
38 S. Ahmad, S. Chaudhary, V. V. Pathak, R. Kothari and V. V. Tyagi, *Renewable Energy*, 2020, **160**, 86–97.
39 E. Safakish, H. Nayebzadeh, N. Saghatoleslami and S. Kazemifard, *Algal Res.*, 2020, **49**, 101949.
40 T. T. Mamo and Y. S. Mekonnen, *Appl. Biochem. Biotechnol.*, 2020, **190**, 1147–1162.